JACS
JOURNAL OF THE AMERICAN CHEMICAL SOCIETY
Article
pubs.acs.org/JACS

Chemoaffinity-Mediated Synthesis of $NaRES_2$-Based Nanocrystals as Versatile Nano-Building Blocks and Durable Nano-Pigments

Yi Ding,‡ Jun Gu,‡ Tao Zhang, An-Xiang Yin, Lu Yang, Ya-Wen Zhang,* and Chun-Hua Yan*

Beijing National Laboratory for Molecular Sciences, State Key Laboratory of Rare Earth Materials Chemistry and Applications, PKU-HKU Joint Laboratory in Rare Earth Materials and Bioinorganic Chemistry, College of Chemistry and Molecular Engineering, Peking University, Beijing 100871, China

Supporting Information

ABSTRACT: In this article, we present a chemoaffinity-mediated synthetic strategy toward trivalent rare earth (RE) sulfides-based nanocrystals with poor affinity between cation and anion (i.e., RE^{3+} and S^{2-}). With the affinity mediation among multiple constituents based on hard and soft acid and base theory, we synthesized a series of monodisperse $NaRES_2$ nanocrystals (RE = La to Lu, Y). The revelation of the nanocrystal growth mechanism from both experimental evidence and crystal structure modeling has enabled a robust control over the sizes and morphologies of the nanocrystals. This principle of chemoaffinity has also promised the synthesis of well-defined but even more complex RE-based hetero-nanostructures (i.e. $NaLaS_2$-Au, Au@$NaLaS_2$, $NaLaS_2$@Ag_2S, Au@$NaLaS_2$@Ag_2S) with tunable optical properties. Furthermore, this synthetic method has yielded durable $NaCeS_2$-based red nano-pigments under ambient conditions, with superior brightness and permeability in polydimethylsiloxane.

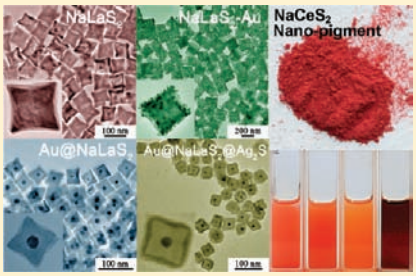

INTRODUCTION

The past two decades of advances in studying colloidal inorganic nanocrystals (NCs)[1−6] have not only opened up new ways to unravel the fundamental questions in synthetic chemistry,[1−6] quantum physics,[7] and crystallography in the nanometer regime,[8−11] but also demonstrated great potential for a broad range of applications spanning optics, electronics, magnetics, photonics, plasmonics, catalysis, biosensing, etc.[1−13] With the development of wet chemistry synthesis, a myriad of NCs have been synthesized, including semiconductor NCs (e.g., groups II−VI,[1,8,14,15] III−V,[16,17]), metal NCs,[18,19] magnetic NCs (especially transition metal-based),[20,21] and rare earth (RE)-based NCs,[22−24] etc., representing different types of nanoscale building blocks. Furthermore, with kinetic and/or thermodynamic control over both solution reactions and NC growth regimes, a plenitude of hybrid NCs constructed from such building blocks have been successfully prepared,[25−31] leading to not only combination of functions of each individual component but also new synergetic effects on material properties due to multicomponent interactions.[25]

The latest great endeavors have been made to promote the research on RE NCs due to their special 4f electron configuration[22,32−37] and promising applications in bioimaging,[38−41] catalysis,[42−44] magnetism,[45,46] etc. So far, a collection of works have demonstrated that the formation of monodisperse RE NCs can be realized and controlled by pyrolysis of precursors in high-boiling-point solvents.[23,24,47−53] We argue that these previous works have revealed the hard and soft acid and base theory (HSAB)[54] to be a valid qualitative principle for understanding the synthesis of RE-based NCs: NCs such as RE oxide (RE_2O_3),[48] RE fluoride (REF_3),[52] RE oxyfluoride (REOF),[47] and sodium RE fluoride ($NaREF_4$)[23,24] are relatively easy to form, whereas NCs containing soft species such as RE oxychloride (REOCl)[49] and RE oxysulfide (RE_2O_2S)[50] tend to form by inclusion of oxygen anions when RE(III) cations react with soft bases such as Cl^- and S^{2-} anions. The synthesis of RE sulfide NCs was realized only in divalent RE elements, such as EuS,[51,53] since the RE(II) ions are softer with larger radius and lower charge. Formation of NCs of RE(III) compounds with only soft base as anions remains a challenge in synthetic chemistry. Furthermore, the difficulty to form trivalent RE sulfides has therefore limited the formation of RE-based hybrid NCs with noble metals as well as with semiconductors, since in solution most of these materials tend to nucleate onto the surface containing soft bases, e.g., S^{2-}, Se^{2-}. This lack of affinity is reflected in the previously reported examples of RE-based hybrid NCs, which resorted to other driving forces, such as ligand interactions,[55] embedment through silica coating[56−58] or PEGylation,[59] biotin−avidin interactions,[60] etc.

Herein, we report a chemoaffinity-mediated synthetic strategy toward trivalent RE sulfides-based NCs, which originally have poor affinity between the cations (i.e., RE^{3+}) and the anions (i.e., S^{2-}). By introducing sodium ions, we have realized the synthesis of $NaRES_2$ (RE = La to Lu, Y) NCs. To the best of our knowledge, this is the first example of trivalent RE sulfide compound NCs synthesized in high-boiling-point organic solvents. Since there is an interesting relationship between the synthetic routes to $NaLaS_2$ NCs and the previously reported La_2O_2S:Na NCs,[61] both crystallographic analysis and

Received: December 9, 2011
Published: January 16, 2012

   dx.doi.org/10.1021/ja211103b | J. Am. Chem. Soc. 2012, 134, 3255−3264

the growth mechanism of these two types of NCs are discussed. Because of the existence of the soft base S^{2-} in the crystal lattice, chemoaffinity dictates that different kinds of RE-based hybrid NCs through both heteronucleation and ion-exchange reaction can also be synthesized: i.e., Au@$NaLaS_2$, $NaLaS_2$−Au, $NaLaS_2$@Ag_2S, Au@$NaLaS_2$@Ag_2S NCs. Being a sodium ion conductor[62] and window material with transmission range from 450 to 2000 nm,[63] the as-formed $NaLaS_2$ shell on the Au core can act as dielectric layer to finely tune the surface plasmon resonance (SPR) frequency of the Au NCs. Because of the 4f→5d electron transition of Ce(III), its sulfides, such as γ-Ce_2S_3[64] and $NaCeS_2$,[65] can serve as oxidation/UV-stable and nontoxic red pigment which is widely used in the fabrication of plastic toys and many other sensitive fields. As synthesized by this chemoaffinity mediation strategy, $NaCeS_2$ NCs with size smaller than the wavelength of red light possess a higher scattering effect, which leads to stronger tinctorial strength and hiding power than for the bulk counterpart.[66] Furthermore, smaller size and long-chain organic capping agents endow the as-synthesized $NaCeS_2$ NCs with better permeability in nonpolar solvent and polymers.[67]

EXPERIMENTAL SECTION

Materials. Oleic acid (OA; 90%, Aldrich), oleylamine (OM; >80%, Acros), 1-octadecene (ODE; >90%, Acros), 1-hexadecylamine (HDA; >92%, Schuchardt), cerium(III) acetate hydrate ($Ce(Ac)_3{\cdot}xH_2O$; 99.9% metals basis, Aldrich), RE oxides (RE_2O_3, RE = La, Pr, Nd, Sm to Lu, Y; >99.99%), sodium hydroxide (NaOH; >96%), sodium oleate (C.P. grade), potassium hydroxide (KOH; A.R. grade), acetylacetone (Hacac; A.R. grade), sublimed sulfur (S; A.R. grade), hydrogen sulfide and nitrogen mixed gas (20% H_2S + 80% N_2; Alpha AeroBrighty), silver nitrate ($AgNO_3$; A.R. grade), chloroauric acid hydrate ($HAuCl_4{\cdot}xH_2O$; >A.R. grade), sodium borohydride ($NaBH_4$; A.R. grade), hexadecyltrimethylammonium bromide (CTAB; >99%), dodecylamine (DDA; >99%), dodecyldimethylammonium bromide (DDAB; >99%, Tokyo Kasei Kogyo Co. Ltd.), 1-docecanethiol (>98%), absolute ethanol (>99.7%), methanol (>99.9%), cyclohexane (>99.5%), toluene (A.R. grade), nitric acid (HNO_3; A.R. grade), ammonia ($NH_3{\cdot}H_2O$; A.R. grade), barium sulfate ($BaSO_4$; A.R. grade), SYLGARD silicone elastomer 184 and the curing agent (Dow Corning Corp.) were used as received.

Synthesis of $NaRES_2$ Nanocrystals (RE = La to Nd, Sm to Tb). Sodium acetylacetonate (Na(acac)) was prepared by following the previously reported procedures.[68] Rare earth acetylacetonate ($RE(acac)_3$, RE = La, Pr to Lu, Y) was prepared by following the procedure described in ref 48. Schlenk line system was utilized under N_2 atmosphere. In a typical synthesis of $NaRES_2$ NCs, $RE(acac)_3$ (RE = La, Pr, Nd, Sm to Tb; 0.5 mmol) or $Ce(Ac)_3$ (0.5 mmol), Na(acac) (4 mmol), S (5 mmol), OA (5 mmol), OM (17 mmol), and ODE (20 mmol) were loaded in a three-neck flask (100 mL) at room temperature. The mixture was heated to 110 °C under vacuum for 20 min to remove water and oxygen and also to form RE-oleate and Na-oleate complexes.[24,47] The mixture was then heated to 315 °C at a rate of 20 °C min^{-1} and then kept for 10 min under N_2. When the reaction was completed, the solution was air-cooled to room temperature. During the cooling of the solution, the residual sodium oleate formed gel under 120 °C. Therefore, 50 mL of ethanol was added into the solution and heated under reflux for 15 min in order to dissolve sodium oleate as well as to precipitate the as-formed NCs from the crude solution. The solution was then centrifuged at 6000 rpm and the supernatant discarded. The as-obtained NCs were washed by ethanol/cyclohexane mixed solution several times before being redispersed in nonpolar organic solvents such as cyclohexane, toluene, and chloroform. Finely adjusting the ratio between sodium precursor and RE precursor while maintaining the other conditions would lead to different sizes and shapes of the $NaRES_2$ NCs. The aforementioned procedure is called method I in the following discussion; size control in the synthesis of the $NaRES_2$ NCs was also realized by (i) using H_2S gas as sulfur precursor instead of sublimed sulfur (method II) and (ii) employing hot-injection method (method III) (for detailed synthetic procedures, refer to Supporting Information (SI)). $NaCe_xLa_{1-x}S_2$ NCs and $KCeS_2$ microcrystals were also synthesized by a similar procedure with corresponding changes in precursors (detailed procedure, refer to SI). For heavy RE (Dy to Lu, Y), $NaRES_2$ NCs could also be synthesized in HDA/ODE mixed solvent when H_2S gas was used as sulfur precursor (detailed procedure, refer to SI).

Synthesis of $NaLaS_2$-Au Hybrid Nanocrystals. The synthetic procedure was conducted in toluene solution. The $NaLaS_2$-Au hybrid NCs with Au deposition onto $NaLaS_2$ surfaces were synthesized through a modification of the procedures for CdSe-Au hybrid NCs developed by Banin and co-workers.[27] First, 0.044 mmol of $NaLaS_2$ NCs was dissolved into 15 mL of toluene. Gold stock solution was prepared by dissolving 0.020 mmol of $HAuCl_4{\cdot}H_2O$, 0.148 mmol of CTAB, and 0.464 mmol of DDA into 10 mL of toluene and sonicating for 5 min. This gold stock solution was then injected dropwisely into the toluene solution of $NaLaS_2$ NCs under vigorous stirring. The as-formed solution was kept for 3−12 h, resulting in different deposition density on the surface of $NaLaS_2$ NCs. Next, 10 mL of ethanol was added to facilitate the precipitation of the as-formed $NaLaS_2$-Au hybrid NCs. The resultant solution was centrifugally separated and redispersed in nonpolar organic solutions such as toluene and cyclohexane.

Synthesis of Au@$NaLaS_2$ Hybrid Nanocrystals. The synthesis of Au@$NaLaS_2$ hybrid NCs was realized in a two-step method. Au NCs were first synthesized through a modification of the method proposed by Klabunde and co-workers[69] (detailed procedure, refer to SI). Next, 0.005 g of the as-formed Au NCs was dissolved into the mixed solution of 0.75 mmol of OM and 0.80 mmol of ODE as stock solution. The synthesis of Au@$NaLaS_2$ hybrid NCs was inspired by the synthetic procedure of Au@PbS NCs developed by Talapin and co-workers.[30] The synthesis was performed by utilizing a Schlenk line system. The three-neck flask was loaded with the same amount of $La(acac)_3$, Na(acac), sublimed sulfur precursors, and the same mixed solution of OA/OM/ODE as in the synthesis of $NaLaS_2$ NCs. After degassing under vacuum at 110 °C for 20 min, the solution was heated to 315 °C under N_2 at a rate of 20 °C min^{-1}. When the reaction temperature reached 315 °C, the Au NCs stock solution was quickly injected into the flask, and the reaction was maintained at 315 °C for 5−20 min. The different reaction times led to different thicknesses of the shell of $NaLaS_2$. The solution turned from dark purple to dark blue within 5 min. The subsequent separation procedure was the same as that used to synthesize $NaLaS_2$ NCs.

Synthesis of $NaLaS_2$@Ag_2S and Au@$NaLaS_2$@Ag_2S Hybrid Nanocrystals. The ion-exchange reaction was used to further synthesize $NaLaS_2$@Ag_2S and Au@$NaLaS_2$@Ag_2S hybrid NCs. The ion-exchange method was a modification of the procedure developed by Alivisatos and co-workers.[70] In a typical synthesis, 0.095 mmol of $NaLaS_2$ NCs was dispersed in 2 mL of toluene; 0.10 mmol of $AgNO_3$ was added into the mixed solution containing 1 mL of methanol and 9 mL of toluene. One milliliter of this stock solution was added dropwise into the toluene dispersion of $NaLaS_2$ NCs. The dispersion turned from white to black instantly upon addition of $AgNO_3$ solution. The synthesis of Au@$NaLaS_2$@Ag_2S was the same except that Au@$NaLaS_2$ NCs were utilized. The dispersion turned from dark blue to black in this case. The exchange reaction could be tuned by differentiating the ratio between $NaLaS_2$ NCs and $AgNO_3$, leading to different thicknesses of the shell of Ag_2S. The separation procedures of the as-formed hybrid NCs were similar to those in the synthesis of $NaLaS_2$-Au hybrid NCs.

Instrumentation. X-ray diffraction (XRD) patterns of the dry powders were characterized on a D/MAX-2000 diffractometer (Rigaku, Japan) with a slit of 1/2° at a scanning speed of 4° min^{-1} using Cu Kα radiation. Samples for transmission electron microscopy (TEM) analysis were prepared by drying a drop of diluted colloidal solution of NCs in either toluene or cyclohexane on copper grids coated by amorphous carbon. TEM, selected area electron diffraction (SAED), high-resolution TEM (HRTEM), high-angle annular dark-

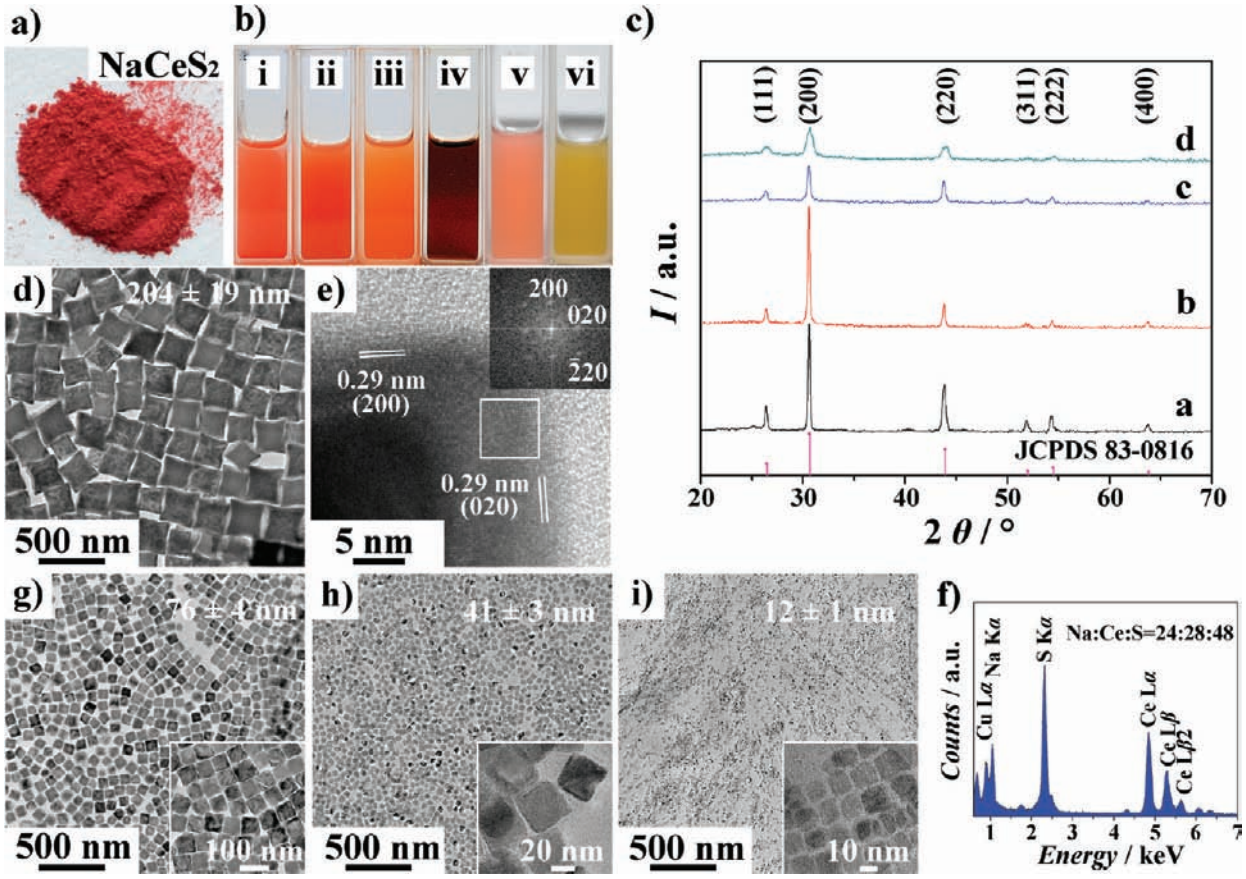

Figure 1. (a) Photograph of red $NaCeS_2$ nanopigment powder in the size of 204 nm; (b) Photographs of dispersions of monodispersed $MRES_2$ (M = Na, K; RE = La, Ce) pigment NCs of different sizes in cyclohexane, from i to vi: 204 nm $NaCeS_2$ (sample A), 76 nm $NaCeS_2$ (sample B), 41 nm $NaCeS_2$ (sample C), 12 nm $NaCeS_2$ (sample D), $NaCe_{0.60}La_{0.40}S_2$, $KCeS_2$, respectively; (c) XRD patterns of differently sized $NaCeS_2$ NCs (samples A–D); TEM images of (d) sample A, (g) sample B, (h) sample C, (i) sample D; the inset is the enlarged TEM image of corresponding sample; (e) HRTEM image of $NaCeS_2$ NCs (sample A), inset is the corresponding FFT pattern; (f) EDX characterization of $NaCeS_2$ NCs (sample A).

field scanning TEM (HAADF-STEM), and energy-dispersive X-ray spectroscopy (EDX) analyses were performed on a FEG-TEM instrument (JEM-2100F, JEOL, Japan) operated at 200 kV. Particle sizes are counted from at least 200 NCs. Samples for scanning electron microscopy (SEM) analysis were prepared by drying a drop of diluted colloid solution on silicon wafers. SEM analyses were performed on a FIB system (FEI Strata DB 235) operated at 15.0 kV. XPS characterizations were performed on an Axis Ultra imaging photoelectron spectrometer (Kratos, Japan). For exact determination of the core level binding energies, the spectrometer was calibrated with C 1s at 284.6 eV. The diffuse reflection spectrum, transmission spectra and absorption spectra at room temperature were taken on a UV-3100 spectrophotometer (Shimadzu, Japan) with an integral detector. Figure S1 in SI shows the schematic of diffuse reflection spectrum and transmission spectra measurements. $BaSO_4$ and absolute cyclohexane were used as reference. The direct transmission spectra can be obtained by deducting scattering transmission spectra from total transmission spectra.[67]

RESULTS AND DISCUSSION

1. Characterization of $NaRES_2$ Nanocrystals. $NaRES_2$ NCs (RE = La to Lu, Y) can be synthesized with the method presented in this article. Herein, a detailed characterization of the as-synthesized red $NaCeS_2$ NCs pigments with different sizes is shown in Figure 1. Samples A–D (corresponding to Figure 1d, g, h, and i, respectively) were synthesized by following methods I, II, and III described in SI. The injection temperatures of samples C and D were 322 and 326 °C, respectively. The diffraction peaks in the XRD pattern shown in Figure 1c confirm the formation of $NaCeS_2$ cubic phase (space group, *Fm*3*m*; JCPDS Card No. 83-0816). The gradual increase in the broadening of the XRD peaks from samples A–D indicates the formation of the $NaCeS_2$ NCs with decreasing sizes. This is in accordance with the TEM observation, which shows that the as-synthesized NCs are highly monodisperse nanocubes with edge lengths of 204 ± 19 (sample A), 76 ± 4 (sample B), 41 ± 3 (sample C), and 12 ± 1 nm (sample D), respectively. Both the HRTEM (Figure 1e) image and the SAED pattern (Figure S2 in SI) indicate that the as-synthesized $NaCeS_2$ NCs are single-crystalline and enclosed mainly by their {200} facets. Further EDX characterization shown in Figure 1f confirmed the stoichiometric composition of the NCs.

$NaLaS_2$ NCs with different sizes and morphologies can also be obtained by changing the concentration of La precursor, as shown in Figure 2a,b. When 0.5 mmol of $La(acac)_3$ was used, concave-shaped $NaLaS_2$ nanocubes with edge length of 68 ± 4 nm would form (Figure 2a and Figure S3 in SI). If the amount of $La(acac)_3$ was reduced to 0.3 mmol, the as-formed $NaLaS_2$ nanocubes were mainly cubic shape with rounded vertices with edge length of 26 ± 2 nm (Figure 2b). The shape evolution from cubes to concave cubes s further illustrated in SI (Figure S4).

The TEM characterizations of the as-formed $NaRES_2$ NCs are shown in Figure S5 in SI. The corresponding XRD patterns shown in Figure S6 in SI are in good agreement with JCPDS

dx.doi.org/10.1021/ja211103b | J. Am. Chem. Soc. 2012, 134, 3255–3264

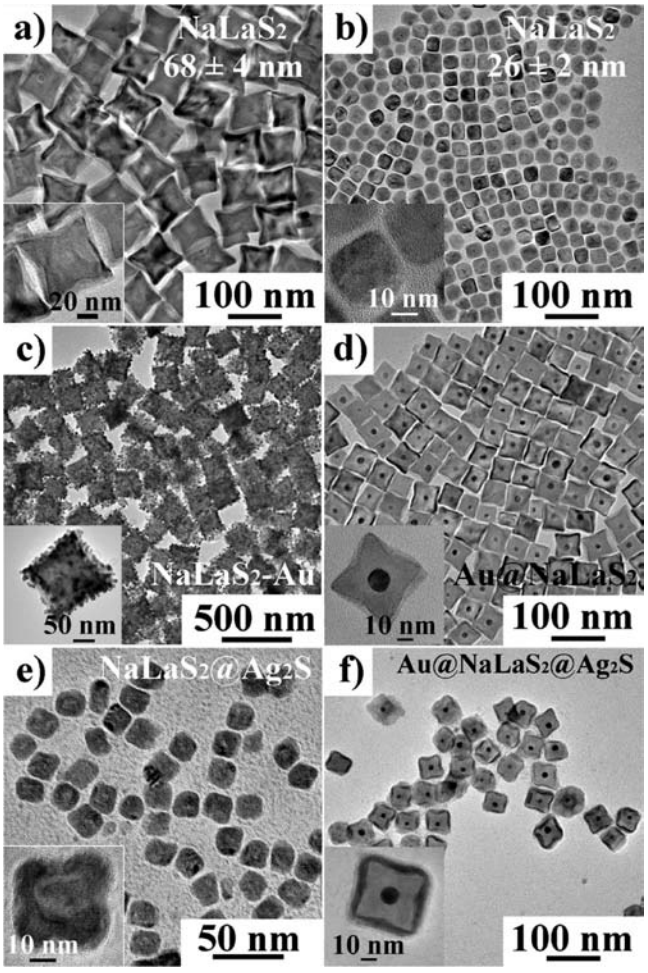

Figure 2. TEM images of (a) 68 nm $NaLaS_2$ NCs, (b) 26 nm $NaLaS_2$ NCs, (c) $NaLaS_2$−Au NCs, (d) Au@$NaLaS_2$ NCs, (e) $NaLaS_2$@Ag_2S NCs, and (f) Au@$NaLaS_2$@Ag_2S NCs. The insets are enlarged pictures of the corresponding NCs.

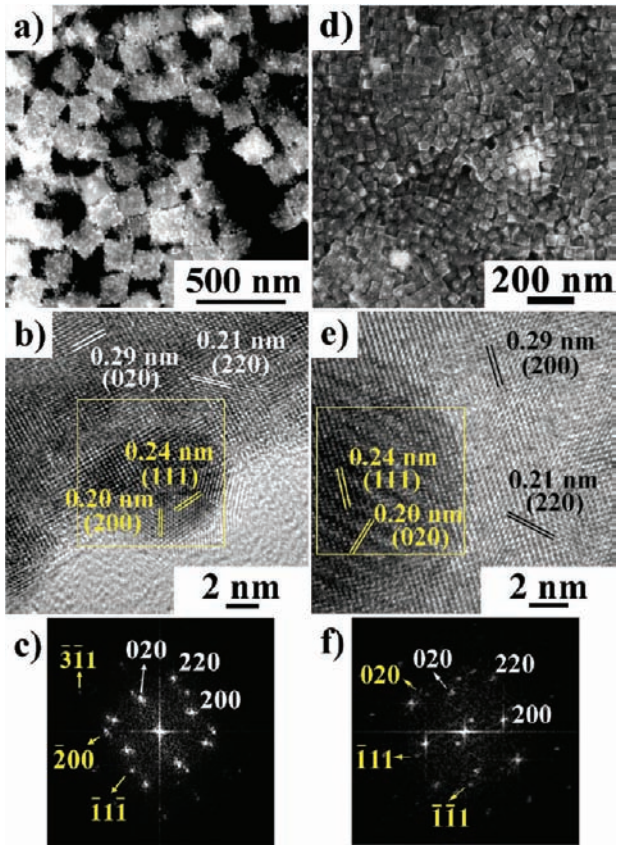

Figure 3. Detailed characterization of $NaLaS_2$-based hybrid NCs: (a) HAADF-STEM image, (b) HRTEM image, and (c) corresponding FFT pattern of $NaLaS_2$-Au NCs, and (d) SEM image, (e) HRTEM image, and (f) FFT pattern of Au@$NaLaS_2$ NCs. The yellow and white (or black) indices in HRTEM and FFT characterization correspond to Au and $NaLaS_2$, respectively.

data, confirming the formation of $NaRES_2$ (cubic phase for RE = La to Nd, space group $Fm3m$; rhombohedral phase for RE = Sm to Lu, Y, space group $R3\bar{m}$). The influence of the lanthanide contraction can be seen in the XRD patterns, with gradual shift of the diffraction peaks to higher anglesalong the RE series (Figure S6 in SI).

2. Characterization of $NaLaS_2$-Based Hybrid NCs. As mentioned in the Experimental Section, different kinds of $NaLaS_2$-based hybrid NCs,including $NaLaS_2$-Au (Figure 2c), Au@$NaLaS_2$ (Figure 2d), $NaLaS_2$@Ag_2S (Figure 2e), and Au@ $NaLaS_2$@Ag_2S (Figure 2f), could be synthesized. As for $NaLaS_2$-Au NCs, the dark-field images of HAADF-STEM and HRTEM and the corresponding fast Fourier transformation (FFT) pattern shown in panels a−c of Figure 3 indicate that the Au NCs (9 ± 1 nm in size) are deposited onto the surface of the $NaLaS_2$ NCs (172 ± 9 nm in size). As shown in both Figures 2c and 3a, Au NCs demonstrated a random distribution over the surface of $NaLaS_2$ NCs, indicating no preferential nucleation positions. The formation of another kind of heterostructured NCs, i.e., Au@$NaLaS_2$ NCs, is also proved by both electron microscopic characterizations (Figures 2d and 3d) and XRD analysis (Figure 4d). The diameter of Au cores is 9 ± 1 nm, and the total edge length is 29 ± 2 nm. A large-scale TEM image (Figure S7 in SI) shows the good dispersibility of Au@$NaLaS_2$ NCs in cyclohexane. It is noteworthy that the $NaLaS_2$ shell on the Au core showed very high monocrystallinity,[71] which can be deduced by the regular cubic shape of the $NaLaS_2$ shell in TEM images and confirmed by both HRTEM and FFT analyses in Figure 3e,f.

Apart from Au@$NaLaS_2$ NCs, the formation of both $NaLaS_2$@Ag_2S NCs (edge length of $NaLaS_2$ core, 19 ± 1 nm) and Au@$NaLaS_2$@Ag_2S (Au core diameter, 14 ± 2 nm; edge length of Au@$NaLaS_2$ core, 38 ± 3 nm) NCs is also confirmed by different characterization methods (Figure 4). The HRTEM image and the corresponding FFT and XRD patterns in Figure 4a,b,d show the formation of Ag_2S layer upon cation exchange. EDX scans of a single $NaLaS_2$@Ag_2S NC were also performed, and a typical result is shown in Figure 4c. The determined mole ratio of Na:La:S:Ag = 6:23:30:41 indicates the existence of the four ingredients in the core−shell particle. HAADF-STEM image of single Au@$NaLaS_2$@Ag_2S NC is shown in Figure 4e (inset), with the corresponding EDX line scan, demonstrating a high level of Ag element enriched on the shell of the NC and Au element enriched in the core, while the counts for La element remains nearly steady inside the NC.

3. Formation Condition and Growth Mechanisms of $NaRES_2$-Based Nanocrystals. Our experiments showed several different aspects of both formation condition and crystal growth process of $NaRES_2$ NCs, i.e., phase transition along RE series, diffusion-controlled shape evolution (Figure S4 in SI), relationship among RE_2O_3, RE_2O_2S, RE_2O_2S:Na, and

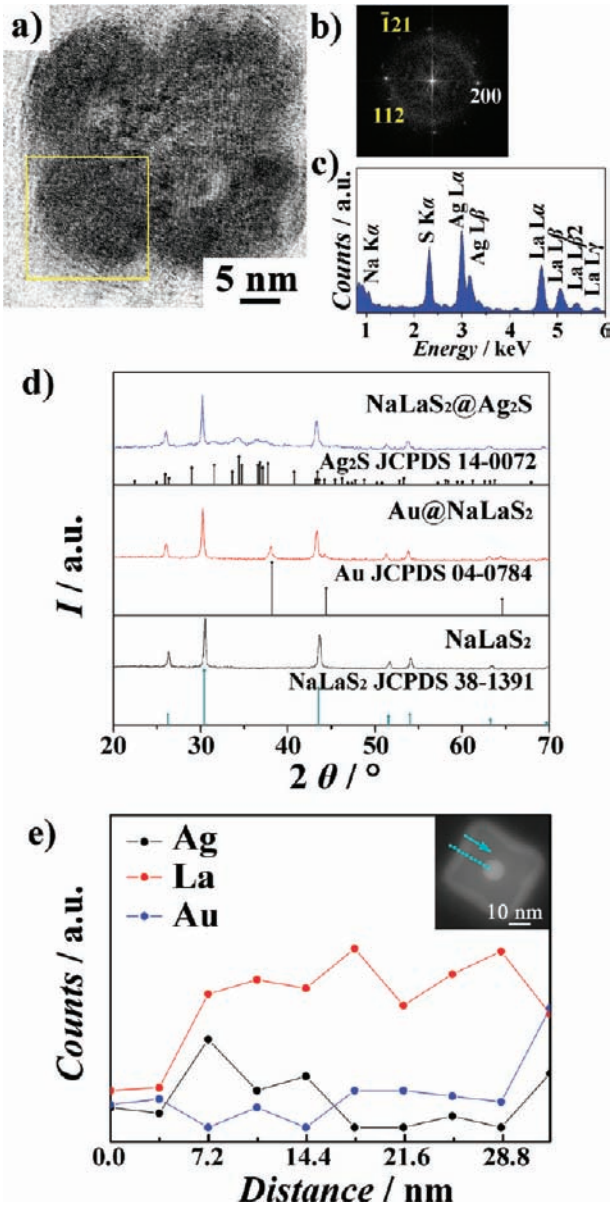

Figure 4. (a) HRTEM image of $NaLaS_2$@Ag_2S NCs. The yellow square is further characterized by FFT analysis shown in panel (b). The yellow and white indices in panel (b) indicate the Fourier-transform diffractogram of Ag_2S and $NaLaS_2$, respectively. (c) Corresponding EDX characterization of the $NaLaS_2$@Ag_2S NCs. (d) Different XRD patterns indicate the formation of $NaLaS_2$ NCs, Au@$NaLaS_2$ NCs and $NaLaS_2$@Ag_2S NCs. (e) Single-particle EDX line scan spectrum with dark-field HAADF-STEM image (inset) of Au@$NaLaS_2$@Ag_2S NCs and the corresponding scan profile and direction.

$NaRES_2$ crystal structures (Figure 5), and size control through different methods (methods I–III described in SI).

Phase Transition of $NaRES_2$ NCs along RE Series. Depending on the ionic radii of RE(III) ions, $NaRES_2$ compounds possess two different crystal structures, i.e., cubic phase and rhombohedral phase. Typically, cubic phase $NaRES_2$ NCs would form when the ionic radius of the RE element is similar to that of sodium ion Na^+, namely, La^{3+}, Ce^{3+}, Pr^{3+}, and Nd^{3+}.[72] The crystal structure of cubic phase $NaRES_2$ can be described as NaCl type, i.e., |AcBaCb| AcBaCb type along the ⟨111⟩ direction, with uppercase A, B, and C representing face-centered close packing (fcc) S^{2-} and lowercase a, b, and c

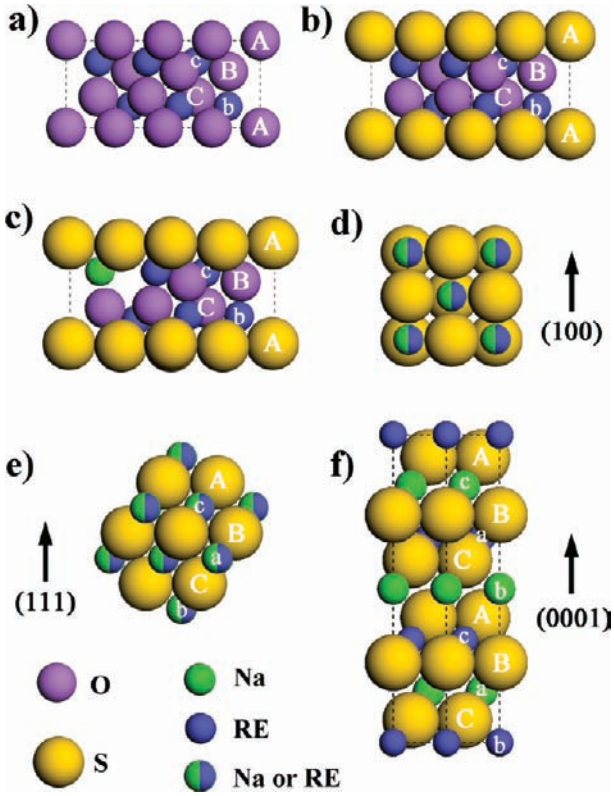

Figure 5. Schematic illustration of different types of lanthanide chalcogenide compounds: (a) hexagonal RE_2O_3, (b) RE_2O_2S, (c) Na-doped RE_2O_2S (sodium ions were found to stabilize the formation of RE_2O_2S NCs, as discussed in detail in ref 61), (d,e) cubic $NaRES_2$, and (f) hexagonal $NaRES_2$. Uppercase letters A, B, and C represent layers of anion ions (i.e., S^{2-} and O^{2-}); lowercase letters a, b, and c represent layers of cation ions (i.e., RE^{3+} or Na^+).

representing fcc of randomly distributed Na^+ or RE^{3+} (Figure 5d,e). The RE(III) ions smaller than Nd^{3+} (RE = Sm to Lu, Y) are also much smaller than Na^+, it is therefore more energetically favorable to form nonrandomly distributed $NaFeO_2$-type crystals, i.e., while maintaining the |AcBaCb AcBaCb| structure, the $NaRES_2$ now possesses three layers of La^{3+} and three layers of Na^+ (represented by the lowercase letters) alternatively sandwiched in the fcc-type S^{2-} layers (represented by the uppercase letters, Figure 5f). The as-synthesized cubic phase $NaRES_2$ NCs ($NaCeS_2$ in Figure 1, $NaLaS_2$ in Figure 2a,b, $NaPrS_2$ and $NaNdS_2$ in Figure S5 in SI) are generally nanocubes bounded by {002} facets, showing this O_h symmetry of the crystals. On the other hand, the rhombohedral-phase $NaRES_2$ NCs (Figure S5 in SI) mainly possess the hexagonal or rhombohedral shapes.

We also found that the formation of $NaRES_2$ NCs became more difficult when RE elements were heavier: while sulfur powder can be used in the synthesis of $NaRES_2$ NCs with light RE (La to Tb), $NaRES_2$ NCs with heavy RE (Y, Dy to Lu) can only be synthesized with H_2S as the sulfurizing agent; the presence of OA would increase the acidity of reaction mixture and inhibit the formation of $NaRES_2$ NCs. This required synthetic condition can be attributed to the fact that, according to HSAB, RE^{3+} ions get harder with smaller radii along RE series, thus the chemoaffinity between RE^{3+} and S^{2-} gets weaker.

Relationship between $NaLaS_2$ NCs and La_2O_2S:Na NCs. Previously, we have reported the formation of ultrathin

dx.doi.org/10.1021/ja211103b | J. Am. Chem. Soc. 2012, 134, 3255–3264

La_2O_2S:Na nanoplates with a diameter of 22 nm, in which the doping of sodium ions into the crystal lattice by replacing lanthanum ions could facilitate the formation of La_2O_2S phase.[61] It is noteworthy that the major difference in synthetic route between $NaLaS_2$ NCs and La_2O_2S:Na NCs is the concentration ratio of the precursors, i.e., $La(acac)_3$, Na(acac), and S in the solution. A typical ratio of precursors in the synthesis of La_2O_2S:Na NCs was Na(acac):$La(acac)_3$:S = 1:1:1 (all precursors are 0.5 mmol while the condition of the mixed solvent was the same as that in the synthesis of $NaLaS_2$ NCs). In the $NaLaS_2$ system, it was found that significantly higher concentrations of Na and S precursors than La precursor can lead to the formation of $NaLaS_2$ NCs, despite the fact that the composition ratio of Na:La:S is 1:1:2 in the compound. Specifically, when the concentration ratio between Na and La was higher than 6:1 (3 mmol:0.5 mmol), only $NaLaS_2$ NCs were formed; when Na:La was between 4:1 (2 mmol:0.5 mmol) and 6:1, the as-synthesized NCs were mixtures of $NaLaS_2$ NCs and La_2O_2S:Na nanoplates (Figure S8a in SI); when Na:La was lower than 4:1, only La_2O_2S:Na nanoplates were formed.[61]

This indicates that the phase transition from La_2O_2S:Na to $NaLaS_2$ is dominated by the chemical potential of Na (μ_{Na}), La (μ_{La}), and S (μ_S) in the reaction solution. Higher μ_S and μ_{Na} are needed to obtain stable $NaLaS_2$ phase. The transport of ions in the diffusion layer of the $NaLaS_2$ NCs might also contribute to the formation of the NCs: as the surfaces of NCs are charged due to polarization or capping, the electrostatic interaction plays its role in attracting monomers to the surface.[73] The monocharged Na^+ ions are subject to smaller attraction force compared to triple-charged La^{3+} ions, so more Na precursors were needed in order to transport same quantity of Na^+ to the crystal surface. Besides this transport requirement, the experimental results also suggested a clear relationship between $NaLaS_2$ and La_2O_2S:Na NCs[61] in their nucleation and growth, and the LaMer[74] model is therefore employed to explain their relative growth mechanisms (Figure 6). For $NaLaS_2$ NCs, compared with La_2O_2S:Na nanoplates, higher concentration of the precursors is required for nucleation, and the formation of much bigger-sized $NaLaS_2$ NCs in less time indicates a bigger gap between the supersaturation concentration and saturation concentration during NC growth.

On the other hand, there is a structural connection among hexagonal La_2O_3, La_2O_2S, La_2O_2S:Na, and $NaLaS_2$: the hexagonal La_2O_3 can be regarded as two layers of La^{3+} cations in three layers of fcc-type O^{2-} anions (|AcBCb|AcBCb type, Figure 5a); in La_2O_2S, the structure is the same as hexagonal La_2O_3, except that the fcc-type anions layers are composed of 1/3 of S^{2-} layers (represented by the uppercase letter A) and 2/3 of O^{2-} layers (represented by the uppercase letters B and C), and the La^{3+} cation layers are sandwiched between one layer of S^{2-} and one layer of O^{2-} (i.e., between A and B or between A and C, Figure 5b); as for La_2O_2S:Na, the dopants of Na^+ randomly replace La^{3+}, causing the formation of $V_O^{\bullet\bullet}$ and facilitating the sulfurization process. During NCs synthesis, the existence of Na^+ stabilizes the La_2O_2S phase, so that one of the three fcc-type O^{2-} anion layers of La_2O_3 can be easily substituted by S (|AcBCb|AcBCb type, Figure 5c); in the case of $NaLaS_2$, with further increased amount of Na^+ and S^{2-}, the sulfurization process goes further, making all three layers of anions change from O^{2-} to S^{2-} while further adding one cation layers between B and C anion layers to balance the charge (Figure 5d–f). The function of the addition of sodium ions can be understood as an adjustment to the chemoaffinity between the cations and the anions in the crystal lattice: since the monovalent sodium ions occupy the position of trivalent RE ions randomly, the hardness of the cations decreases accordingly, thus facilitating the formation of sulfides containing RE ions.

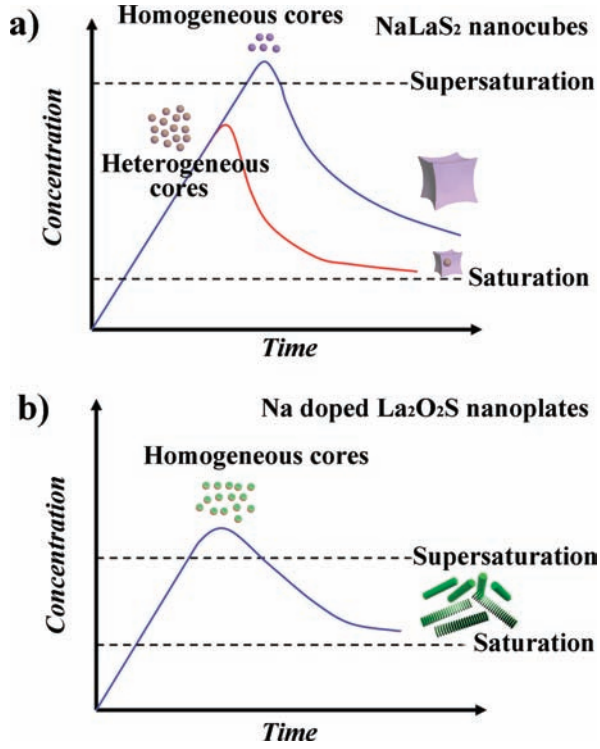

Figure 6. LaMer schemes of (a) $NaLaS_2$ NCs and (b) Na-doped La_2O_2S NCs.

Control over Sizes of $NaCeS_2$ NCs. As shown in Figure 1, we have devised different synthesis procedure to realize the control over sizes of the $NaCeS_2$ NCs, so that the edge lengths could be finely tuned from 10 to 200 nm. $NaCeS_2$ NCs with edge lengths of 204 nm would form within 10 min at 315 °C when elementary sulfur was used as the sulfurizing agent. Since the $NaCeS_2$ NCs grows relatively fast in the solution, simply decreasing the reaction time was hard to controllably synthesize NCs with edge lengths smaller than 100 nm. In this case, methods II and III (listed in SI) are employed in order to increase the number of nucleus formed in solution[75] so as to generate NCs with edge lengths smaller than 100 nm. In method II, sublimed sulfur powder was replaced by H_2S gas as the sulfurizing agent. As reported by Ozin and co-workers,[76] when elementary sulfur was used as sulfurizing agent in the synthesis of metal sulfide NCs, the active component of sulfur existed in solution was the as-generated H_2S. On the other hand, H_2S gas was also used directly as the sulfurizing agent in the synthesis of CdSe@CdS core–shell NCs.[77] With the direction injection of H_2S gas, the effective concentration of H_2S in OM solution would be higher, leading to more nuclei formed in solution. The edge length of the $NaCeS_2$ NCs would therefore decrease, since the same amount of monomer was consumed by more nuclei. In a typical synthesis (sample B), $NaCeS_2$ with edge length of 76 ± 4 nm was successfully prepared (Figure 1g). In method III, hot injection of precursors was utilized to further increase the number of nuclei. By this method, we have realized the synthesis of smaller NCs with

dx.doi.org/10.1021/ja211103b | J. Am. Chem. Soc. 2012, 134, 3255–3264

edge lengths of 41 ± 3 and 12 ± 1 nm when the injection temperature was 322 and 326 °C, respectively (Figure 1h,i).

Construction of Hybrid NCs Based on $NaLaS_2$. It is generally accepted that for heterogeneous nucleation, the surfaces of the two materials should have high affinity (thus low surface tension), since thermodynamically the changes in Gibbs energy of forming a particle homogeneously and heterogeneously can be respectively written as

$$\Delta G_{\text{homo}} = V\Delta G_{\text{v}} + A_{\text{s-l}}\gamma_{\text{s-l}} \quad (1)$$

$$\Delta G_{\text{hetero}} = V\Delta G_{\text{v}} + A_{\text{s1-l}}\gamma_{\text{s1-l}} + A_{\text{s1-s2}}\gamma_{\text{s1-s2}} - A_{\text{s2-l}}\gamma_{\text{s2-l}} \quad (2)$$

where V is the newly formed volume of the particles, ΔG_v is the change in Gibbs energy per volume, A is the newly formed surface area of the particles, γ is the interface energy either between solid and liquid (subscript s−l) or between two types of solids (subscript s−s). Therefore, the interface energy between two materials ($\gamma_{\text{s1-s2}}$) is the key factor in the formation of heterostructures, and it should be small enough that the energy barrier of heterogeneous nucleation is lower thus more favorable than homogeneous nucleation. In our system, since S^{2-} in $NaLaS_2$ NCs has strong affinity toward Au NCs, the interface energy between the two materials (i.e., $\gamma_{\text{NaLaS2-Au}}$) is relatively small. So the surface of Au NCs can be the nucleation points for $NaLaS_2$, which leads to the formation of Au@$NaLaS_2$ hybrid NCs. We found 315 °C to be the optimal temperature for the injection of Au NCs. Though the decomposition of $La(acac)_3$ occurs above 310 °C, it takes several minutes for the monomers to reach supersaturation. Under this condition, the instant introduction of Au nuclei facilitates the formation of $NaLaS_2$ NCs. This affinity of $NaLaS_2$ surface to Au atoms is also the reason for the formation of $NaLaS_2$−Au heterostructure. As a result, mild reduction of $HAuCl_3$ in the presence of $NaLaS_2$ NCs can leads to heteronucleation of Au on the surface of $NaLaS_2$.

Kinetically, since $NaLaS_2$ has relatively high growth rate and big gap between saturation and supersaturation concentrations, the introduction of Au NCs would therefore facilitate the growth process of $NaLaS_2$ NCs (red line in the LaMer diagram in Figure 6a). This is proven in the subsequent experiment with precursors ratio of Na(acac):$La(acac)_3$ = 6:1 (3 mmol: 0.5 mmol) while maintaining all other parameters of the synthesis. While under standard procedure, this concentration would lead to the mixture of La_2O_2S and $NaLaS_2$ NCs, with the introduction of Au NCs, the as-formed NCs were solely Au@$NaLaS_2$ (Figure S8b in SI). This phenomenon is in great accordance with the prediction given by the relationship of La_2O_2S and $NaLaS_2$ NCs shown in the LaMer diagram (Figure 6). Since the population of Au@$NaLaS_2$ NCs was totally determined by the number of Au cores introduced externally, which was much larger than the number of homocores that could form without the introduction of heterocores, the size of the Au@$NaLaS_2$ NCs are significantly smaller than $NaLaS_2$ NCs synthesized under same condition, as shown in Figures 2d and 6a. Furthermore, the control over the amount of Au nuclei can serve to intentionally tune the thickness of the $NaLaS_2$ layer from 6.0 to 10.0 nm: specifically, when more Au NCs were introduced into the solution, thinner $NaLaS_2$ layers were generated (Figure S9 and Table S1 in SI).

Since the cations of most sulfide semiconductors are soft acid according to HSAB theory, and Na and La are both hard acids, we can make profit of their difference in hardness to perform ion exchange reactions so as to generate other complex heterostructures. Herein, we used toluene solution of $AgNO_3$ to synthesize both $NaLaS_2$@Ag_2S and Au@$NaLaS_2$@Ag_2S NCs (Figures 2 and 4). The corresponding reactions can be summarized as

$$NaLaS_2 + Ag^+ \rightarrow Ag_2S + Na^+ + La^{3+} \quad (3)$$

It is also noteworthy that Na^+ ions are much lighter than La^{3+} ions and have the same valence as Ag^+ ions. In this case, Na^+ ions ought to possess higher mass transport rate than La^{3+} ions do in the ion-exchange reaction in the solution. As a result, the amount of Na^+ exchanged by Ag^+ is greater than that of La^{3+}, as indicated by the measured EDX ratio (i.e., molar ratio of Na:La:S:Ag = 6:23:30:41) for the $NaLaS_2$@Ag_2S NCs. More interestingly, the thickness of Ag_2S layer can be tuned by adjusting the ratio between $NaLaS_2$ (as well as Au@$NaLaS_2$) NCs and $AgNO_3$ (Figure S10 in SI). Since the strong chemoaffinity between S^{2-} and Au as well as Ag^+, $NaLaS_2$ can be effectively used as a platform to construct complex hybrid NCs through direct heteronucleation and cation exchange, thus enriching the family of RE-based hybrid NCs.

Since $NaLaS_2$ NCs are used as IR window materials with the refractive index of 1.74 ± 0.02 and with great transmission for wavelengths longer than 450 nm,[63] the $NaLaS_2$ shell can lead to a red shift (from 525 to 615 nm) of the SPR frequency of Au cores (Figure 7).[30] The Ag_2S shell on the Au@$NaLaS_2$ NCs can further lead to a broadening and a slight red-shift (from 615 to 622 nm) of the absorption peak in UV−vis spectrum.[78]

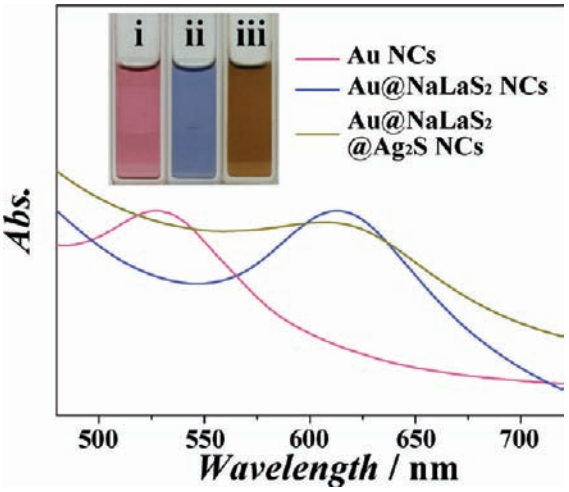

Figure 7. Absorption spectra and corresponding photos of toluene dispersions of (i) Au NCs (pink line), (ii) Au@$NaLaS_2$ NCs (blue line), and (iii) Au@$NaLaS_2$@Ag_2S NCs (dark yellow line).

4. $NaCeS_2$ NCs as Inorganic Nano-Pigments and the Size Dependency of Its Color. *Basic Colorimetric Characterization of $NaCeS_2$ NCs.* It was shown that the as-prepared NCs maintain a similar chroma compared to their bulk counterparts and possess a higher brightness at the same time. Figure 8a shows the diffuse reflection spectrum of $NaCeS_2$ nanocubes with edge lengths of 204 nm. The main absorption peak around λ = 500 nm, which is responsible for the red color of the as-prepared $NaCeS_2$ NCs, is ascribed to the 4f→5d transition of Ce(III). From Figure 8a we can calculate the color coordinates of the as-prepared $NaCeS_2$ NCs: L^* =

dx.doi.org/10.1021/ja211103b | J. Am. Chem. Soc. 2012, 134, 3255−3264

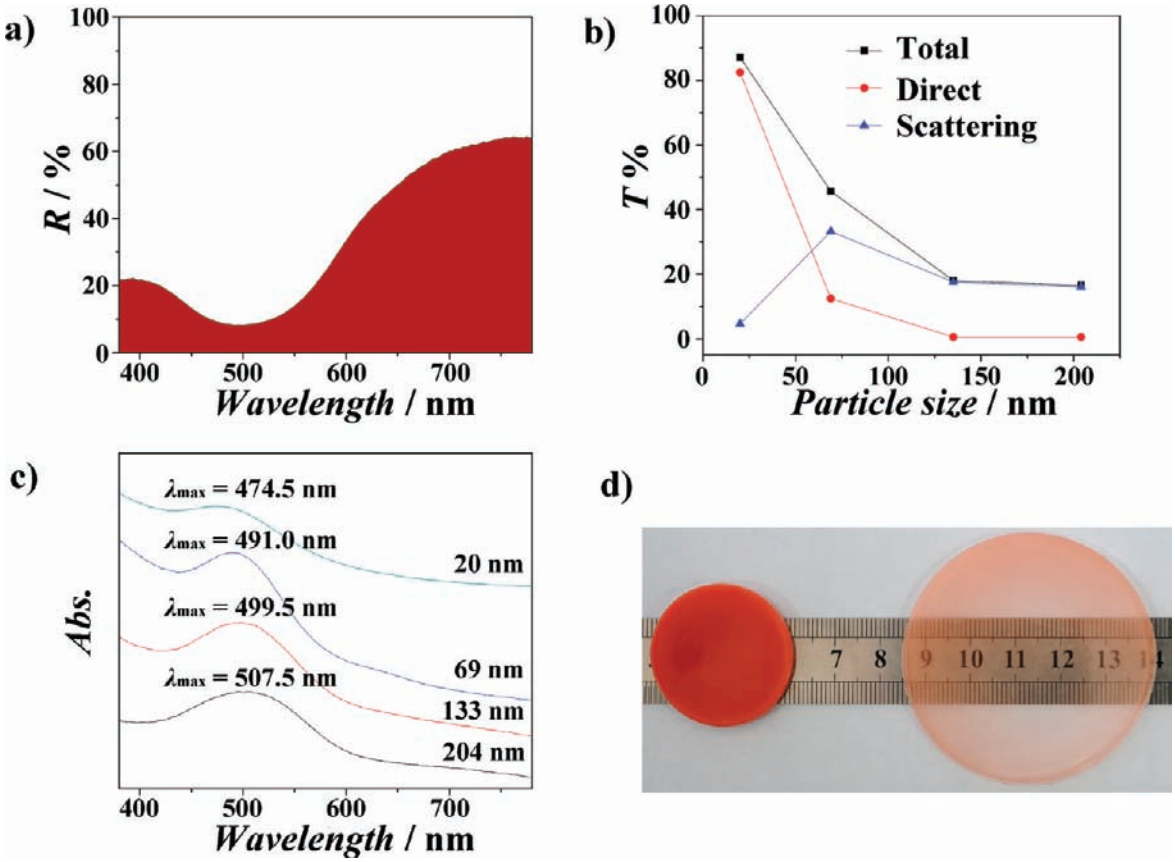

Figure 8. (a) Diffuse reflection spectrum of $NaCeS_2$ nanocubes with side length of 204 nm. (b) Transparency of the cyclohexane dispersion of $NaCeS_2$ NCs that depends on the side length of the nanocubes. Red light with wavelength of 750 nm was used as the test light, and all the dispersion samples were diluted to the same concentration of 0.5 mg/mL. (c) UV−vis spectra of the cyclohexane dispersions of $NaCeS_2$ NCs of different sizes. (d) Photograph that shows the $NaCeS_2$ nanocubes/PDMS composite materials.

54.0, a^* = 41.1, b^* = 18.7, C^* = 45.1. The color coordinates were calculated employing the CIE 1976 L^* a^* b^* (CIELAB) procedure. The yield of red color is mainly described by the parameter a^*: the more positive the a^* value, the redder is the hue. Therefore, the as-prepared $NaCeS_2$ NCs produced a redder hue compared with bulk $NaCeS_2$ red pigment (L^* = 43.8, a^* = 38.6, b^* = 23.0, C^* = 44.9).[65]

Further tuning of the color can be realized by replacing a part of the Ce(III) with La(III) to form $NaCe_xLa_{1-x}S_2$ NCs. Since $NaLaS_2$ NCs show only white hue, this doping method can be utilized to tune the chroma and brightness of the red-colored $NaCeS_2$ nano-pigments. For instance, compared with $NaCeS_2$ NCs, $NaCe_{0.60}La_{0.40}S_2$ NCs possess a lower chroma (C^* = 42.1) and a higher brightness (L^* = 62.2) (Figure 1b-v and Figure S11 and Table S2 in SI). Similarly, if Na(acac) was replaced by K(acac), yellow-colored $KCeS_2$ microcrystals could also be synthesized (Figure 1b-vi and Figure S12 and Table S3 in SI).

Size-Dependent Properties of $NaCeS_2$ Inorganic Nano-Pigment. According to XPS and UV−vis absorption characterization, the as-prepared $NaCeS_2$ NCs with edge lengths larger than 70 nm were stable in air, while smaller $NaCeS_2$ NCs were subject to gradual oxidation and discoloring (Figures S13 and S15 in SI). Figure 8b shows the transparency of the cyclohexane dispersion of $NaCeS_2$ NCs depends on their edge lengths (Figure S14 in SI shows the transmission spectra of these four samples.) Both the direct transparency and the total transparency have an increasing trend as the particle size decreases, and when the edge length of the NCs is smaller than 20 nm, the NCs dispersion is almost transparent. Interestingly, the sizes of the $NaCeS_2$ NCs influence not only the transparency but also the color of their dispersions. Figure 8c shows the UV−vis spectra of the cyclohexane dispersions of $NaCeS_2$ NCs of different sizes. The decreasing of particle sizes leads to a blue-shift of the main absorption peak around λ = 500 nm, which is ascribed to the 4f→5d transition of Ce(III), indicating a slight change of the crystal field around Ce(III) ions because of the high sensitivity of 5d electron orbital to the surrounded neighboring ions.[79] This blue shift of the main absorption peak therefore leads to a tiny increase in the transparency of the green and yellow light in the range of 500−600 nm.

Furthermore, the as-formed $NaCeS_2$ NCs can be used to fabricate red-colored polydimethylsiloxane (PDMS) (Figure 8d; for fabrication procedure, refer to SI). The PDMS monolith shown on the left of Figure 8d contains 0.24 wt % of $NaCeS_2$ NCs with edge length of 204 nm, while the right one contains 0.054 wt % of $NaCeS_2$ NCs with edge length of 69 nm.

■ CONCLUSIONS

We have demonstrated that the chemoaffinity among different elements plays a key role in the synthesis of NCs, especially trivalent RE-based NCs. Guided by this principle, we have realized the synthesis of $NaRES_2$ NCs with high monodispersity and controllable sizes through the co-thermolysis of precursors in the mixed solution of OA/OM/ODE. The as-

synthesized NCs exhibit diffusion-controlled shape evolution, leading to the formation of concave nanocubes under certain synthetic conditions. The synthesis of $NaRES_2$ has also enabled us to further examine the interesting connections among different RE chalcogenide NCs (e.g., RE_2O_3, RE_2O_2S, and $NaRES_2$), through both growth mechanism and crystal structure analysis. The analysis allows us to elucidate the formation of these NCs with different chemoaffinity among various ingredient elements. Different types of $NaRES_2$-based heterostructures were also synthesized. Among these NCs, $NaCeS_2$ NCs can serve as a nontoxic and durable inorganic nano-pigment with better performance than its bulk counterpart; $NaLaS_2$ NCs is a transparent window material with high refractive index and can be used to construct complex functional hybrid NCs. In all, the chemoaffinity-mediated synthetic strategy demonstrated in this work could be utilized to guide the synthesis of a wide variety of homo- and heterostructured inorganic NCs, especially NCs composed of cations and anions of much different hardness.

■ ASSOCIATED CONTENT

Supporting Information

More experimental details, schematic illustration of the diffuse reflection spectrum, total transmission spectrum and scattering transmission spectrum, more TEM images, and results of EDX, XRD, and XPS analyses. This material is available free of charge via the Internet at http://pubs.acs.org.

■ AUTHOR INFORMATION

Corresponding Author

ywzhang@pku.edu.cn; yan@pku.edu.cn

Author Contributions

‡These authors contributed equally.

Notes

The authors declare no competing financial interest.

■ ACKNOWLEDGMENTS

This work was supported by the NSFC (grant nos. 21025101, 20871006, and 20821091). Y.W.Z.. particularly appreciates the financial aid of China National Funds for Distinguished Young Scientists from the NSFC.

■ REFERENCES

(1) Murray, C. B.; Norris, D. J.; Bawendi, M. G. *J. Am. Chem. Soc.* **1993**, *115*, 8706.
(2) Park, J.; An, K. J.; Hwang, Y. S.; Park, J. G.; Noh, H. J.; Kim, J. Y.; Park, J. H.; Hwang, N. M.; Hyeon, T. *Nat. Mater.* **2004**, *3*, 891.
(3) Wang, X.; Zhuang, J.; Peng, Q.; Li, Y. D. *Nature* **2005**, *437*, 121.
(4) Park, J.; Joo, J.; Kwon, S. G.; Jang, Y.; Hyeon, T. *Angew. Chem., Int. Ed.* **2007**, *46*, 4630.
(5) Tao, A. R.; Habas, S.; Yang, P. *Small* **2008**, *4*, 310.
(6) Xia, Y.; Xiong, Y.; Lim, B.; Skrabalak, S. E. *Angew. Chem., Int. Ed.* **2009**, *48*, 60.
(7) Borys, N. J.; Walter, M. J.; Huang, J.; Talapin, D. V.; Lupton, J. M. *Science* **2010**, *330*, 1371.
(8) Peng, X. G.; Manna, L.; Yang, W. D.; Wickham, J.; Scher, E.; Kadavanich, A.; Alivisatos, A. P. *Nature* **2000**, *404*, 59.
(9) Murray, C. B. *Science* **2009**, *324*, 1276.
(10) Schliehe, C.; Juarez, B. H.; Pelletier, M.; Jander, S.; Greshnykh, D.; Nagel, M.; Meyer, A.; Foerster, S.; Kornowski, A.; Klinke, C.; Weller, H. *Science* **2010**, *329*, 550.
(11) Yin, Y.; Alivisatos, A. P. *Nature* **2005**, *437*, 664.
(12) Kotov, N. A. *Science* **2010**, *330*, 188.
(13) Talapin, D. V.; Lee, J. S.; Kovalenko, M. V.; Shevchenko, E. V. *Chem. Rev.* **2010**, *110*, 389.
(14) Chen, O.; Yang, Y.; Wang, T.; Wu, H.; Niu, C.; Yang, J.; Cao, Y. C. *J. Am. Chem. Soc.* **2011**, *133*, 17504.
(15) Gaponik, N.; Talapin, D. V.; Rogach, A. L.; Hoppe, K.; Shevchenko, E. V.; Kornowski, A.; Eychmuller, A.; Weller, H. *J. Phys. Chem. B* **2002**, *106*, 7177.
(16) Guzelian, A. A.; Katari, J. E. B.; Kadavanich, A. V.; Banin, U.; Hamad, K.; Juban, E.; Alivisatos, A. P.; Wolters, R. H.; Arnold, C. C.; Heath, J. R. *J. Phys. Chem.* **1996**, *100*, 7212.
(17) Nozik, A. J.; Micic, O. I. *MRS Bull.* **1998**, *23*, 24.
(18) Skrabalak, S. E.; Au, L.; Li, X.; Xia, Y. *Nat. Protoc.* **2007**, *2*, 2182.
(19) Sau, T. K.; Murphy, C. J. *J. Am. Chem. Soc.* **2004**, *126*, 8648.
(20) Sun, S. H.; Murray, C. B.; Weller, D.; Folks, L.; Moser, A. *Science* **2000**, *287*, 1989.
(21) Kim, D.; Lee, N.; Park, M.; Kim, B. H.; An, K.; Hyeon, T. *J. Am. Chem. Soc.* **2008**, *131*, 454.
(22) Heer, S.; Kompe, K.; Gudel, H. U.; Haase, M. *Adv. Mater.* **2004**, *16*, 2102.
(23) Boyer, J.-C.; Cuccia, L. A.; Capobianco, J. A. *Nano Lett.* **2007**, *7*, 847.
(24) Mai, H. X.; Zhang, Y. W.; Si, R.; Yan, Z. G.; Sun, L. D.; You, L. P.; Yan, C. H. *J. Am. Chem. Soc.* **2006**, *128*, 6426.
(25) Costi, R.; Saunders, A. E.; Banin, U. *Angew. Chem., Int. Ed.* **2010**, *49*, 4878.
(26) Milliron, D. J.; Hughes, S. M.; Cui, Y.; Manna, L.; Li, J. B.; Wang, L. W.; Alivisatos, A. P. *Nature* **2004**, *430*, 190.
(27) Mokari, T.; Rothenberg, E.; Popov, I.; Costi, R.; Banin, U. *Science* **2004**, *304*, 1787.
(28) Choi, J.-S.; Jun, Y.-W.; Yeon, S.-I.; Kim, H. C.; Shin, J.-S.; Cheon, J. *J. Am. Chem. Soc.* **2006**, *128*, 15982.
(29) Cozzoli, P. D.; Pellegrino, T.; Manna, L. *Chem. Soc. Rev.* **2006**, *35*, 1195.
(30) Lee, J.-S.; Shevchenko, E. V.; Talapin, D. V. *J. Am. Chem. Soc.* **2008**, *130*, 9673.
(31) Lee, J.-S.; Bodnarchuk, M. I.; Shevchenko, E. V.; Talapin, D. V. *J. Am. Chem. Soc.* **2010**, *132*, 6382.
(32) Wang, F.; Liu, X. *Chem. Soc. Rev.* **2009**, *38*, 976.
(33) Feng, W.; Sun, L.-D.; Zhang, Y.-W.; Yan, C.-H. *Coord. Chem. Rev.* **2010**, *254*, 1038.
(34) Wang, G.; Peng, Q.; Li, Y. *Acc. Chem. Res.* **2011**, *44*, 322.
(35) Stouwdam, J. W.; Hebbink, G. A.; Huskens, J.; van Veggel, F. *Chem. Mater.* **2003**, *15*, 4604.
(36) Wang, F.; Deng, R.; Wang, J.; Wang, Q.; Han, Y.; Zhu, H.; Chen, X.; Liu, X. *Nat. Mater.* **2011**, *10*, 968.
(37) Haase, M.; Schafer, H. *Angew. Chem., Int. Ed.* **2011**, *50*, 5808.
(38) Wang, F.; Banerjee, D.; Liu, Y.; Chen, X.; Liu, X. *Analyst* **2010**, *135*, 1839.
(39) Boyer, J.-C.; Manseau, M.-P.; Murray, J. I.; van Veggel, F. C. J. M. *Langmuir* **2010**, *26*, 1157.
(40) Chen, Z.; Chen, H.; Hu, H.; Yu, M.; Li, F.; Zhang, Q.; Zhou, Z.; Yi, T.; Huang, C. *J. Am. Chem. Soc.* **2008**, *130*, 3023.
(41) Chatterjee, D. K.; Gnanasammandhan, M. K.; Zhang, Y. *Small* **2010**, *6*, 2781.
(42) Mai, H. X.; Sun, L. D.; Zhang, Y. W.; Si, R.; Feng, W.; Zhang, H. P.; Liu, H. C.; Yan, C. H. *J. Phys. Chem. B* **2005**, *109*, 24380.
(43) Wang, R.; Crozier, P. A.; Sharma, R.; Adams, J. B. *Nano Lett.* **2008**, *8*, 962.
(44) Li, B.; Metiu, H. *J. Phys. Chem. C* **2011**, *115*, 18239.
(45) Selinsky, R. S.; Han, J. H.; Perez, E. A. M.; Guzei, I. A.; Jin, S. *J. Am. Chem. Soc.* **2010**, *132*, 15997.
(46) Liu, Q.; Sun, Y.; Li, C.; Zhou, J.; Li, C.; Yang, T.; Zhang, X.; Yi, T.; Wu, D.; Li, F. *ACS Nano* **2011**, *5*, 3146.
(47) Du, Y.-P.; Zhang, Y.-W.; Yan, Z.-G.; Sun, L.-D.; Yan, C.-H. *J. Am. Chem. Soc.* **2009**, *131*, 16364.
(48) Si, R.; Zhang, Y. W.; You, L. P.; Yan, C. H. *Angew. Chem., Int. Ed.* **2005**, *44*, 3256.
(49) Du, Y.-P.; Zhang, Y.-W.; Sun, L.-D.; Yan, C.-H. *J. Am. Chem. Soc.* **2009**, *131*, 3162.

(50) Zhao, F.; Yuan, M.; Zhang, W.; Gao, S. *J. Am. Chem. Soc.* **2006**, *128*, 11758.
(51) Mirkovic, T.; Hines, M. A.; Nair, P. S.; Scholes, G. D. *Chem. Mater.* **2005**, *17*, 3451.
(52) Zhang, Y. W.; Sun, X.; Si, R.; You, L. P.; Yan, C. H. *J. Am. Chem. Soc.* **2005**, *127*, 3260.
(53) Zhao, F.; Sun, H. L.; Su, G.; Gao, S. *Small* **2006**, *2*, 244.
(54) Pearson, R. G. *Science* **1966**, *151*, 172.
(55) Shen, J.; Sun, L.-D.; Zhang, Y.-W.; Yan, C.-H. *Chem. Commun.* **2010**, *46*, 5731.
(56) Li, Z. Q.; Zhang, Y.; Jiang, S. *Adv. Mater.* **2008**, *20*, 4765.
(57) Zhang, F.; Braun, G. B.; Shi, Y.; Zhang, Y.; Sun, X.; Reich, N. O.; Zhao, D.; Stucky, G. *J. Am. Chem. Soc.* **2010**, *132*, 2850.
(58) Hu, D.; Chen, M.; Gao, Y.; Li, F.; Wu, L. *J. Mater. Chem.* **2011**, *21*, 11276.
(59) Zhang, H.; Li, Y.; Ivanov, I. A.; Qu, Y.; Huang, Y.; Duan, X. *Angew. Chem., Int. Ed.* **2010**, *49*, 2865.
(60) Wang, L. Y.; Yan, R. X.; Hao, Z. Y.; Wang, L.; Zeng, J. H.; Bao, H.; Wang, X.; Peng, Q.; Li, Y. D. *Angew. Chem., Int. Ed.* **2005**, *44*, 6054.
(61) Ding, Y.; Gu, J.; Ke, J.; Zhang, Y.-W.; Yan, C.-H. *Angew. Chem. Int. Ed.* **2011**, *50*, 12330.
(62) Masuda, H.; Fujino, T.; Sato, N.; Yamada, K. *Mater. Res. Bull.* **1999**, *34*, 1291.
(63) Isaacs, T. J.; Hopkins, R. H.; Kramer, W. E. *J. Electron. Mater.* **1975**, *4*, 1181.
(64) Perrin, M. A.; Wimmer, E. *Phys. Rev. B* **1996**, *54*, 2428.
(65) Aubert, M.; Macaudiere, P. U.S. Patent 6,221,473, April 24, 2001.
(66) Hund, Z. *Angew. Chem., Int. Ed.* **1981**, *20*, 723.
(67) Rangappa, D.; Naka, T.; Kondo, A.; Ishii, M.; Kobayashi, T.; Adschiri, T. *J. Am. Chem. Soc.* **2007**, *129*, 11061.
(68) Charles, R. G. *Org. Synth.* **1959**, *39*, 61.
(69) Prasad, B. L. V.; Stoeva, S. I.; Sorensen, C. M.; Klabunde, K. J. *Langmuir* **2002**, *18*, 7515.
(70) Son, D. H.; Hughes, S. M.; Yin, Y. D.; Alivisatos, A. P. *Science* **2004**, *306*, 1009.
(71) Zhang, J.; Tang, Y.; Lee, K.; Ouyang, M. *Science* **2010**, *327*, 1634.
(72) Shannon, R. D. *Acta Crystallogr., Sect. A* **1976**, *32*, 751.
(73) Wang, F.; Han, Y.; Lim, C. S.; Lu, Y.; Wang, J.; Xu, J.; Chen, H.; Zhang, C.; Hong, M.; Liu, X. *Nature* **2010**, *463*, 1061.
(74) Lamer, V. K.; Dinegar, R. H. *J. Am. Chem. Soc.* **1950**, *72*, 4847.
(75) Shevchenko, E. V.; Talapin, D. V.; Schnablegger, H.; Kornowski, A.; Festin, O.; Svedlindh, P.; Haase, M.; Weller, H. *J. Am. Chem. Soc.* **2003**, *125*, 9090.
(76) Thomson, J. T., J. W.; Nagashima, K.; Macdonald, P. M.; Ozin, G. A. *J. Am. Chem. Soc.* **2011**, *133*, 5036.
(77) Mekis, I.; Talapin, D. V.; Kornowski, A.; Haase, M.; Weller, H. *J. Phys. Chem. B* **2003**, *107*, 7454.
(78) Yang, J.; Ying, J. Y. *Chem. Commun.* **2009**, *45*, 3187.
(79) Henderson, B.; Imbusch, G. *Optical Spectroscopy of Inorganic Solids*; Clarendon Press: Oxford, 1989; p 396.